J Digit Imaging (2016) 29:388–393
DOI 10.1007/s10278-015-9856-7

# Computer-Aided Diagnosis Scheme for Distinguishing Between Benign and Malignant Masses in Breast DCE-MRI

**Emi Honda**[1,3] · **Ryohei Nakayama**[2] · **Hitoshi Koyama**[1] · **Akiyoshi Yamashita**[1]

Published online: 21 December 2015


**Abstract** Our purpose in this study was to develop a computer-aided diagnosis (CAD) scheme for distinguishing between benign and malignant breast masses in dynamic contrast material-enhanced magnetic resonance imaging (DCE-MRI). Our database consisted 90 DCE-MRI examinations, each of which contained four sequential phase images; this database included 28 benign masses and 62 malignant masses. In our CAD scheme, we first determined 11 objective features of masses by taking into account the image features and the dynamic changes in signal intensity that experienced radiologists commonly use for describing masses in DCE-MRI. Quadratic discriminant analysis (QDA) was employed to distinguish between benign and malignant masses. As the input of the QDA, a combination of four objective features was determined among the 11 objective features according to a stepwise method. These objective features were as follows: (i) the change in signal intensity from 2 to 5 min; (ii) the change in signal intensity from 0 to 2 min; (iii) the irregularity of the shape; and (iv) the smoothness of the margin. Using this approach, the classification accuracy, sensitivity, and specificity were shown to be 85.6 % (77 of 90), 87.1 % (54 of 62), and 82.1 % (23 of 28), respectively. Furthermore, the positive and negative predictive values were 91.5 % (54 of 59) and 74.2 % (23 of 31), respectively. Our CAD scheme therefore exhibits high classification accuracy and is useful in the differential diagnosis of masses in DCE-MRI images.

**Keywords** Computer-aided diagnosis · Mass · DCE-MRI

✉ Emi Honda
emi.jrc.med@gmail.com

[1] Department of Radiology, Japanese Red Cross Medical Center, 4-1-22 Hiroo, Shibuya-ku, Tokyo 150-8935, Japan

[2] Department of Radiology, Mie University School of Medicine, 2-174 Edobashi, Tsu 514-8507, Japan

[3] Graduate School of Health Science, Suzuka University of Medical Science, 1000-1 Kishioka-cho, Suzuka 510-0293, Japan

## Introduction

Dynamic contrast material-enhanced magnetic resonance imaging (DCE-MRI) for breasts has become an established method not only in the preoperative diagnosis of the extent a cancer but also in the detection of an early cancer [1–4]. Breast DCE-MRI has a higher sensitivity than conventional mammography, which is the standard screening modality. Especially in dense breasts, the sensitivity has been improved from the range of 33–59 % with mammography to 71–94 % with DCE-MRI [5–7]. However, breast DCE-MRI suffers from several limitations. The specificity of breast DCE-MRI, which is typically between 67 and 72 %, is lower than that of mammography. Such a low specificity results in a larger number of false positives and higher biopsy rates [8–10]. Furthermore, DCE-MRI requires a significant amount of time for image interpretation.

Computer-aided diagnosis (CAD) is one solution for overcoming these limitations [11]. CAD is defined as a diagnostic method wherein radiologists use the results analyzed by a computer as a "second opinion." In fact, CAD schemes for DCE-MRI images have been developed in many studies [12–17]. In a breast DCE-MRI examination, cancer patterns tend to show rapid initial enhancement, followed by a washout or a plateau in signal intensity over time [18]. Therefore, CAD schemes for breast DCE-MRI often focus on a lesion's dynamic changes in signal intensity on the basis of a contrast agent. Some of those CAD schemes were developed to help identify potentially cancerous regions in breast DCE-MRI

images and to bring them to the attention of radiologists as detection aids. However, a breast DCE-MRI examination is usually performed after an abnormal region is detected by mammography or other modalities. In other words, most lesions have already been detected by the time DCE-MRI is performed. Therefore, we believe that a high-performance CAD scheme is desirable in clinical practice, even if it specializes as a differential diagnosis aid. In order to classify suspicious lesions accurately, it is also necessary to assess not only the signal intensity, but also image features, such as a lesion's shape and margins. To this end, in this study, we develop a CAD scheme for distinguishing between benign and malignant masses by considering the dynamic changes in signal intensity as well as the image features in breast DCE-MRI images.

## Materials and Methods

The use of the following database was approved by the Institutional Review Board at the Japanese Red Cross Medical Center.

### Materials

Our database consisted of 90 DCE-MRI examinations—each of which contained four sequential phase images—that were performed at the Japanese Red Cross Medical Center from 2010 to 2014. These images were obtained a 3.0 T MR scanner (Achieva 3.0 T X-series, Philips Healthcare, Best, Netherlands) from 90 patients (mean age: 56.7 ± 16.7 years; range: 25–86 years) with a mass whose effective diameter was greater than 5 mm. All masses (mean diameter: 19.6 ± 16.2 mm; range: 5–87 mm) underwent core-needle biopsy and/or surgical specimen. They included 28 benign masses and 62 malignant masses (32 invasive ductal carcinomas and 30 ductal carcinomas in situ).

After the injection of Gd-DTPA (Bayer Schering Pharma AG, Berlin, Germany), a contrast agent at a dose of 0.2 mmol for every kg of body weight, and an intravenous saline flush of 30–40 ml at the same flow rate of 1.5 ml/s, three post-contrast series of 3D MRI scans and data acquisitions were sequentially performed after a duration of 1, 2, and 5 min. Fat-saturated T1-weighted 3D images (eTHRIVE: enhanced-T1 High Resolution Isotropic Volume Excitation) were obtained before and after the injection. The imaging parameters of repetition time (TR), echo time (TE), and flip angle (FA) were 4.0 ms, 2.0 ms, and 20°, respectively. Figure 1 shows an example of DCE-MRI images with a malignant mass. The one pre-contrast and three post-contrast series generated images with a spatial resolution of $0.66 \times 0.66 \times 1.0$ mm$^3$, with a data matrix of $512 \times 512$ pixels. Four image scan series each consisted of 150 image slices.

### Segmentation of Mass

The initial enhancement phase usually refers to an increase in signal intensity within the first 2 min after contrast injection [18, 19]. Therefore, for the segmentation of a mass region, the rectangular region of interest (ROI), which included an entire mass, was selected manually on the DCE-MRI image after 2 min by an experienced radiological technologist. The ROI included three groups which consisted of the mass region, breast tissue, and adipose tissue. The mass region had higher signal intensity than non-mass tissues on the DCE-MRI image after 2 min, as shown in Fig. 1. Two threshold values for separating those three groups were determined automatically by applying Otsu's method [20, 21], which is based on the signal intensity used to the set ROI. Additionally, a gray-level threshold technique with a higher threshold value was employed to segment the mass region from the ROI on the DCE-MRI image after 2 min. The region in each DCE-MRI image that corresponded to the segmented mass at 2 min was also defined as a mass region for each phase at 0 (i.e., pre-contrast), 1, and 5 min.

### Extraction of Objective Features

We determined 11 objective features of a mass by taking into account the image features and the dynamic changes in signal intensity that experienced radiologists commonly use for describing masses in DCE-MRI images. These objective features were as follows: (1) the roundness of the shape; (2) the irregularity of the shape; (3) the smoothness of the margin; (4) the irregularity of the margin; (5) the extent of distribution toward the nipple; (6) the heterogeneity of the enhancement pattern; (7) the degree of rim enhancement; (8) the change in signal intensity from 0 to 1 min; (9) the change in signal intensity from 1 to 2 min; (10) the change in signal intensity from 0 to 2 min; and (11) the change in signal intensity from 2 to 5 min. Objective features 1–7, which are concerned with the image features, were extracted from the DCE-MRI images at 2 min, that is because BI-RADS recommends a morphologic evaluation at the early phase within 2 min [18, 19].

#### *Roundness of the Shape*

The area of the mass was defined as the number of pixels within a segmented mass, whereas the maximum length of the mass was defined as the longest distance between any two points on the edge of the segmented mass. The roundness of the shape was determined as follows:

$$\text{roundness of the shape} = \frac{(\text{maximum length})^2}{\text{area}} \times \frac{\pi}{4}. \quad (1)$$

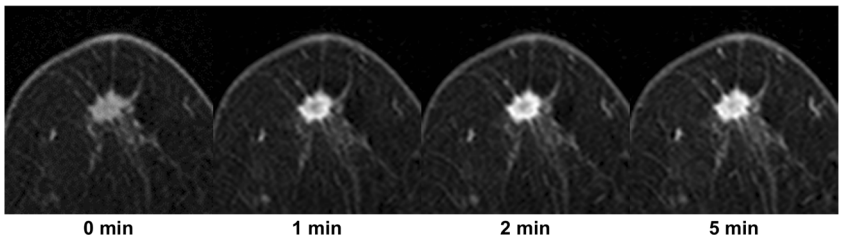


**Fig. 1** Example of dynamic contrast material-enhanced magnetic resonance imaging (DCE-MRI) images with a malignant mass after a duration of 0, 1, 2, and 5 min

*Irregularity of the Shape*

The perimeter of the mass was measured by adding the distances between each adjoining pair of pixels along the edge of the segmented mass. The irregularity of the shape was determined as follows:

$$\text{irregularity of the shape} = \frac{(\text{perimeter})^2}{\text{area}} \times \frac{1}{4\pi}. \quad (2)$$

*Smoothness of the Margin*

The smallest convex hull containing the segmented mass was determined in the segmented image. The smoothness of the margin was defined as the ratio between the area of the mass and that of the convex hull.

*Irregularity of the Margin*

The diameter of a circle with the same area as the segmented mass was given by:

$$\text{diameter of a circle with the same area} = \sqrt{\frac{4 \times \text{area}}{\pi}}. \quad (3)$$

The irregularity of the margin was determined as:

$$\text{degree of irregularity of the margin} = 1 - \frac{\text{diameter} \times \pi}{\text{perimeter}}. \quad (4)$$

*Extent of Distribution Toward the Nipple*

The center of the nipple was first marked by an experienced radiological technologist, whereas the center of the segmented mass was determined automatically. A straight line connecting the center of the nipple with the center of the segmented mass was defined as the directional axis of the nipple. We evaluated the angle (ranging from −90° to 90°) between the directional axis of the nipple and the major axis of the ellipse with the same second moment of area as the segmented mass. The extent of distribution toward the nipple was then determined as:

$$\text{Extent of distribution toward the nipple} = 1 - \frac{|\text{angle}|}{90^\circ}. \quad (5)$$

*Heterogeneity in the Enhancement Pattern*

The relative standard deviations of signal intensities (pixel values) were measured within the segmented masses on DCE-MRI images at 0, 1, 2, and 5 min. The heterogeneity in the enhancement pattern of the mass was simply defined as the highest relative standard deviation.

*Degree of Rim Enhancement*

The inside band was defined as the inside region with a width of 3 pixels along the outline of the mass region. The center region was then defined as the portion of the segmented mass that excluded the inside band. The mean values of the signal intensities in the inside band and in the center region were measured on DCE-MRI images at 0, 1, 2, and 5 min. The ratio of the mean value in the inside band divided by that in the center region was then measured at 0, 1, 2, and 5 min. The degree of rim enhancement was given by the highest ratio obtained.

*Change in Signal Intensity*

The mean values of signal intensity were measured within the segmented masses on DCE-MRI images at 0 and 1 min. The change in signal intensity from 0 to 1 min was determined by the difference between the mean values at 0 and 1 min. In the same way, we determined the change in signal intensity from 1 to 2 min, from 0 to 2 min, and from 2 to 5 min.

**Classification Scheme**

Quadratic discriminant analysis (QDA) was employed for distinguishing between benign and malignant masses in breast DCE-MRI images. The QDA was composed of a discriminant function based on the combination of the objective features that provided the best discrimination between the two groups. The objective features used for the QDA were selected from the 11 objective features according to a stepwise method

based on Wilks's lambda [22, 23]. The stepwise method first selects the objective feature with the lowest Wilks's lambda for entry into the discriminant function. The objective feature is then selected such that the overall Wilks's lambda is minimized in combination with the selected feature. This procedure is repeated until the overall Wilks's lambda does not decrease in combination with the selected features. A leave-one-out testing method [24] was used for the training and testing of the QDA. In this method, the training was carried out for all but one of the cases in the database; the case not used for training was used for testing with the trained QDA. This procedure was repeated until every case in our database had been used once.

## Results

Table 1 shows the results of tests for univariate equality of group means for each of the 11 objective features. The Wilks's lambda for the change in signal intensity from 2 to 5 min was smaller than that of any other feature. This result indicates that this objective feature exhibited the largest discrepancy between benign and malignant groups. On the other hand, the roundness of shape had the largest Wilks's lambda and did not satisfy the significance level (i.e., $P = 0.052$). Accordingly, this feature exhibited a large amount of overlap between the benign and malignant groups.

Four objective features used for the QDA were selected from the 11 objective features with the stepwise method based on the Wilks's lambda. These features were as follows, taken in order of their entry into the discriminant function: (i) the change in signal intensity from 2 to 5 min; (ii) the change in signal intensity from 0 to 2 min; (iii) the irregularity of the shape; and (iv) the smoothness of the margin. All of the four objective features had small Wilks's lambda values and satisfied the significance level (i.e., $P < 0.05$).

Figure 2 shows the relationship between the change in signal intensity from 2 to 5 min and the change in signal intensity from 0 to 2 min. For benign cases, both of these changes in signal intensity tended to be larger than those for malignant cases. Figure 3 shows the relationship between the irregularity of the shape and the smoothness of the margin. The irregularity of the shape for malignant cases appeared to be larger than that for benign cases, whereas the smoothness of the margin for malignant cases tended to be smaller than that for benign cases.

Table 2 shows the computerized classification results with the QDA using the four objective features. The classification accuracy, sensitivity, and specificity were 85.6 % (77 of 90), 87.1 % (54 of 62), and 82.1 % (23 of 28), respectively. The positive and negative predictive values were 91.5 % (54 of 59) and 74.2 % (23 of 31), respectively.

**Table 1** Results of tests for univariate equality of group means in each of the 11 objective features

| Objective Features | Wilks's lambda | *P* value |
|---|---|---|
| Roundness of the shape | 0.958 | 0.052 |
| Irregularity of the shape | 0.931 | 0.013 |
| Smoothness of the margin | 0.907 | 0.004 |
| Irregularity of the margin | 0.889 | 0.001 |
| Extent of distribution toward the nipple | 0.956 | 0.047 |
| Heterogeneity of the enhancement pattern | 0.957 | 0.050 |
| Degree of rim enhancement | 0.949 | 0.032 |
| Change in signal intensity from 0 to 1 min | 0.947 | 0.030 |
| Change in signal intensity from 1 to 2 min | 0.865 | <0.001 |
| Change in signal intensity from 0 to 2 min | 0.884 | 0.001 |
| Change in signal intensity from 2 to 5 min | 0.854 | <0.001 |

## Discussion

The dynamic change in signal intensity over time has often been used in previous studies [12, 14–17]. In order to evaluate the contribution of the image features in distinguishing between benign and malignant masses, the objective features used for the QDA were selected from only four objective features (i.e., features 8–11) regarding the dynamic changes in signal intensity by the stepwise method. Using the QDA based on the change in signal intensity from 0 to 2 min and

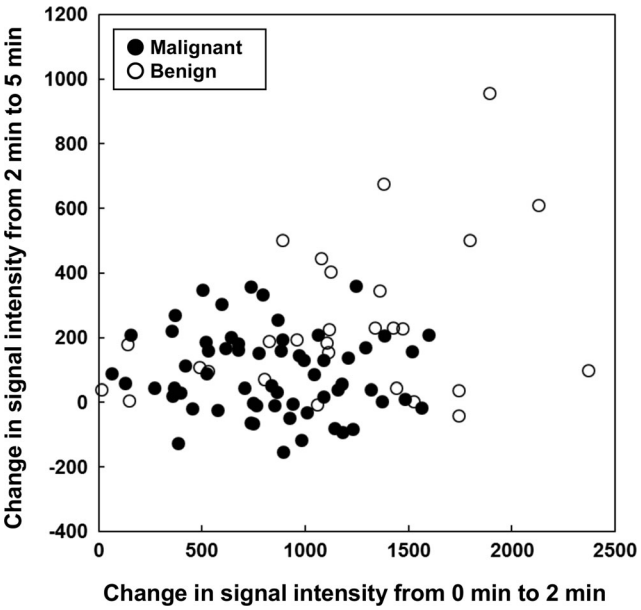


**Fig. 2** Relationship between the changes in signal intensity from 2 to 5 min and from 0 to 2 min

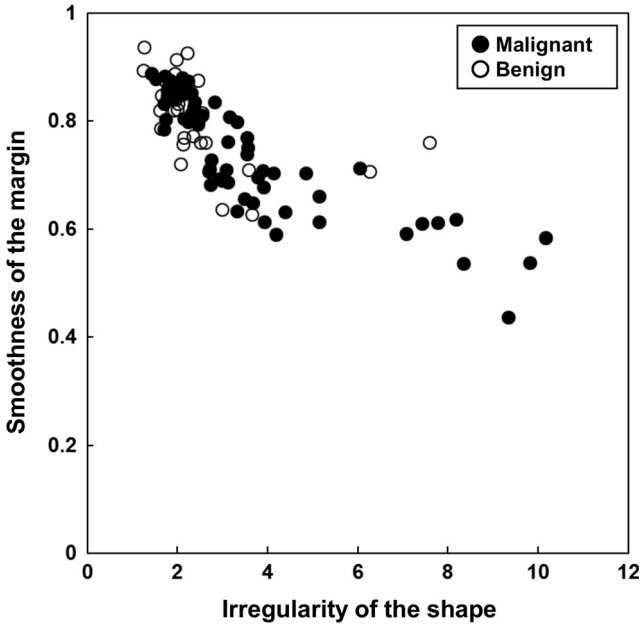


**Fig. 3** Relationship between the smoothness of the margin and the irregularity of the shape

from 2 to 5 min, the classification accuracy, sensitivity, and specificity were 72.2 % (65 of 90), 77.4 % (48 of 62), and 60.7 % (17 of 28), respectively. The positive and negative predictive values were 81.4 % (48 of 59) and 54.8 % (17 of 31), respectively. All results were lower than those obtained with the QDA based on the four objective features selected from the image features and the dynamic changes in signal intensity. This implies that the combination of the image features and the dynamic changes in signal intensity could make a significant contribution in distinguishing between benign and malignant masses.

As a further step in evaluating the usefulness of the stepwise method, we employed a QDA with all 11 objective features in order to distinguish between benign and malignant masses. The classification accuracy, sensitivity, and specificity were 73.3 % (66 of 90), 77.5 % (48 of 62), and 64.3 % (18 of 28), respectively. The positive and negative predictive values were 82.8 % (48 of 58) and 56.3 % (18 of 32), respectively. All results were lower than those obtained with the QDA based on the four objective features selected from the 11 objective features according to the stepwise method. This implies that the stepwise method was indeed useful in selecting features as the inputs of the QDA.

**Table 2** Computerized classification results of the quadratic discriminant analysis (QDA) based on the four objective features selected according to the stepwise method

| | Computer output | |
|---|---|---|
| | Malignant | Benign |
| Malignant (62) | 87.1 % (54/62) | 12.9 % (8/62) |
| Benign (28) | 17.8 % (5/28) | 82.1 % (23/28) |

With our CAD scheme, the classification accuracy, sensitivity, and specificity were 85.6 %, 87.1 %, and 82.1 %, respectively. These results were comparable to the performance of radiologists in the context of differential diagnosis in DCE-MRI examinations [5–10]. Although the classification accuracy of our CAD scheme might have to be further improved in order to aid experienced radiologists, it could nevertheless be useful for less experienced radiologists. Our CAD scheme can output not only the classification results but also the objective features used in making that classification (i.e., the image features and the dynamic changes in signal intensity). In clinical practice, the availability of these objective features would allow radiologists to objectively assess features of the images and to reduce interobserver variability in diagnostic results.

There were some limitations to this study. More specifically, the rectangular ROI was chosen manually in the segmentation of the mass by an experienced radiological technologist. Accordingly, we can expect some variation among the location and the size of such ROIs. As a result, the objective features extracted from the segmented mass would vary because the mass region is segmented on the basis of the threshold value that is determined automatically from the ROI. Therefore, the classification performance of our CAD scheme might vary as the ROI is altered. Another limitation was the fact that there was an imbalance in database between benign and malignant masses. We believe the classification performance of our CAD scheme would not change greatly even if we balance the number of benign masses with malignant masses.

Further study is required to assess the usefulness of our CAD scheme in an observer study and clinical trial.

## Conclusion

We developed a CAD scheme for distinguishing between benign and malignant masses in breast DCE-MRI images by using a combination of the dynamic changes in signal intensity and the image features of the lesion. Our CAD scheme for distinguishing between benign and malignant masses exhibits high classification accuracy and can be useful in the differential diagnosis of masses in DCE-MRI images. In a future study, we plan to improve performance of the CAD scheme by introducing texture features which can analyze tissue structures of mass.

**Acknowledgments** We are grateful to Dr. Ichirou Suzuki, Deputy Chief of the Japanese Red Cross Medical Center, for his useful comments.

**Compliance with Ethical Standards**

**Conflicts of Interest** The authors declare that they have no competing interests.

## References

1. Preda P, Turetschek K, Daldrup H: The choice of region of interest measures incontrast-enhanced magnetic resonance image characterization of experimental breast tumors. Investig Radiol 40:349–354, 2005
2. Warner E, Messersmith H, Causer P, Eisen A, Shumak R, Plewes D: Systematicreview: using magnetic resonance imaging to screen women at high risk for breast cancer. Ann Intern Med 148:671–679, 2008
3. Sardanelli F, Fausto A, Esseridou A, Leo GD, Kirchin MA: Gadobenate dimeglu-mine as a contrast agent for dynamic breast magnetic resonance imaging: effect of higher initial enhancement thresholds on diagnostic performance. Investig Radiol 43:236–242, 2008
4. Pinker K, Grabner G, Bogner W, Gruber S, Szomolanyi P, Trattnig S, et al: A combined high temporal and high spatial resolution 3 Tesla MR imaging protocol for the assessment of breast lesions: initial results. Investig Radiol 44:553–558, 2009
5. Leach MO, Boggis CR, Dixon AK, et al: Screening with magnetic resonance imaging and mammography of a UK population at high familial risk of breast cancer: a prospective multicentre cohort study (MARIBS). Lancet 365:1769–1778, 2005
6. Kuhl CK, Schrading S, Leutner CC, et al: Mammography, breast ultrasound, and magnetic resonance imaging for surveillance of women at high familial risk for breast cancer. J Clin Oncol 23: 8469–8476, 2005
7. Sardanelli F, Podo F, D'Agnolo G, et al: Multicenter comparative multimodality surveillance of women at genetic-familial high risk for breast cancer (HIBCRIT study): interim results. Radiology 242: 698–715, 2007
8. Bluemke DA, Gatsonis CA, Chen MH, DeAngelis GA, DeBruhl N, Harms S, Heywang-Kobrunner SH, Hylton N, Kuhl CK, Lehman C, Pisano ED, Causer P, Schnitt SJ, Smazal SF, Stelling CB, Weatherall PT, Schnall MD: Magnetic resonance imaging of the breast prior to biopsy. JAMA 292:2735–2742, 2004
9. Peters NH, Borel Rinkes IH, Zuithoff NP, Mali WP, Moons KG, Peeters PH: Meta-analysis of MR imaging in the diagnosis of breast lesions. Radiology 246:116–124, 2008
10. Hrung JM, Sonnad SS, Schwartz JS, Langlotz CP: Accuracy of MR imaging in the work-up of suspicious breast lesions: a diagnostic meta-analysis. Acad Radiol 6:387–397, 1999
11. Doi K: Computer-aided diagnosis in medical imaging: historical review, current status and future potential. Comput Med Imaging Graph 31(4–5):198–211, 2007
12. Chen W, Giger ML, Bick U, Newstead GM: Automatic identification and classification of characteristic kinetic curves of breast lesions on DCE-MRI. Med Phys 33(8):2878–2887, 2006
13. Yang Q, Li L, Zhang J, Shao G, Zheng B: A computerized global MR image feature analysis scheme to assist diagnosis of breast cancer: a preliminary assessment. Eur J Radiol 83(7):1086–1091, 2014
14. Yang Q, Li L, Zhang J, Shao G, Zhang C, Zheng B: Computer-aided diagnosis of breast DCE-MRI images using bilateral asymmetry of contrast enhancement between two breasts. J Digit Imaging 27(1):152–160, 2014
15. Rakoczy M, McGaughey D, Korenberg MJ, Levman J, Martel AL: Feature selection in computer-aided breast cancer diagnosis via dynamic contrast-enhanced magnetic resonance images. J Digit Imaging 26(2):198–208, 2013
16. Agliozzo S, De Luca M, Bracco C, Vignati A, Giannini V, Martincich L, Carbonaro LA, Bert A, Sardanelli F, Regge D: Computer-aided diagnosis for dynamic contrast-enhanced breast MRI of mass-like lesions using a multiparametric model combining a selection of morphological, kinetic, and spatiotemporal features. Med Phys 39(4):1704–1715, 2012
17. Lee SH, Kim JH, Cho N, Park JS, Yang Z, Jung YS, Moon WK: Multilevel analysis of spatiotemporal association features for differentiation of tumor enhancement patterns in breast DCE-MRI. Med Phys 37(8):3940–3956, 2010
18. American College of Radiology: Breast imaging reporting and data system (BI-RADS), 5th edition: American College of Radiology, 2013
19. Agrawal G, Su MY, Nalcioglu O, Feig SA, Chen JH: Significance of breast lesion descriptors in the ACR BI-RADS MRI lexicon. Cancer 115(7):1363–1380, 2009. doi:10.1002/cncr.24156
20. Otsu N: A Threshold Selection Method from Gray-Level Histograms. IEEE Trans Syst Man Cybern 9(1):62–66, 1979
21. Liao P-S, Chen T-S, Chung P-S: A Fast Algorithm for Multilevel Thresholding. J Inf Sci Eng 17(5):713–727, 2001
22. Gilhuijs KG, Giger ML, Bick U: Computerized analysis of breast lesions in three dimensions using dynamic magnetic-resonance imaging. Med Phys 25(9):1647–1654, 1998
23. Chen W, Giger ML, Lan L, Bick U: Computerized interpretation of breast MRI: investigation of enhancement-variance dynamics. Med Phys 31(5):1076–1082, 2004
24. Kuncheva LI: Combining Pattern Classifiers: Methods and Algorithms. Wiley, New York, 2004